ISSN 1840-4855
e-ISSN 2233-0046

Original scientific article
http://dx.doi.org/10.70102/afts.2026.1835.598

MECHANICAL ANALYSIS OF STRESS AND DEFORMATION IN LITHIUM BATTERY ELECTRODES DURING CHARGE–DISCHARGE CYCLES

Israa Meften Hashim[1*]

[1*]*Lecturer, College of Nursing, University of Al-Qadisiyah, Al-Qadisiyah, Iraq.*
e-mail: israa.meften@qu.edu.iq, orcid: https://orcid.org/0000-0003-1848-3912

Received: January 21, 2026; Revised: March 05, 2026; Accepted: April 22, 2026; Published: May 29, 2026

SUMMARY

Problem: Lithium-ion batteries are normally inhibited by mechanical degradation under the influence of diffusion that leads to rapid charging of the batteries. The non-uniform lithium concentration gradients, which trigger internal strain, bending, and interfacial failure, contribute to this problem in thick, porous electrodes. While these risks are well-known, there remains a critical gap in existing research for a macro-scale framework that can link practical fabrication parameters to mechanical stability in a computationally efficient way. Methodology: To bridge this gap, developed a coupled chemo-thermo -mechanical macro-scale model designed to quantify electrode stability during cycling. This model is a combination of the second law of Fick, wherein eigenstrain is caused by lithiation, and the elastic-viscoplastic deformation is considered, but the thermal effects are also considered. Also tested the model using a synthetic dataset, the interaction between electrode thickness (50–200 5 C) and the charging rates (0.5 C–5 C), and discretized the model with finite differentiation. Results: Results indicate that peak von Mises stress increases nonlinearly with both C-rate and electrode thickness. At charging rates above 2–3C, peak stress is more than 60% higher than quasi-static values. Thermal coupling further amplifies peak stress by 10–20%, while an ablation study confirms that viscoelastic relaxation is critical, as its removal increases predicted peak stress by 32%. Conclusion: The model provides a computationally efficient screening tool for optimizing electrode layouts such as thickness and porosity before undergoing rigorous micro-scale simulations. By utilizing the Damköhler number and a specialized fracture index, the framework successfully identifies mechanically safe operating windows to mitigate interfacial delamination during fast-charging protocols.

Key words: *battery mechanics, lithiation-induced stress, porous electrode, deformation, fast charging c-rate, chemo-mechanical coupling, electrode curvature.*

INTRODUCTION

Modern electric cars, large-scale energy storage systems, and portable electronic gadgets all rely on lithium-ion batteries, which must now be able to withstand continuous use under demanding charge-discharge cycles [16]. Quick charging is quickly becoming one of the most important performance goals among these needs. SHI is aware that the cyclability, safety, and service life of electrode materials are affected by the large mechanical stresses caused by quick Li insertion-extraction.

There is no uniform distribution of lithium ions across the electrode thickness while fast-charging. As a result of limited diffusion kinetics, large concentration gradients develop in thick porous electrodes. The volumetric expansion of the active material is caused by changes in the gas compositions, such as partial pressure or molar fraction. However, this expansion is physically restricted by the structure of the composite electrode and the current collector. As a result, internal stress fields, bending deformation, and shear stresses at interfaces are produced by heterogeneous eigenstrains [14]. Binder deterioration, particle debonding, delamination, and rapid capacity fading are all results of mechanical reactions like these.

To knowledge, this is the first experimental operando measurement of diffusion-induced stress that reveals its nonlinear scaling with respect to charging rate and electrode thickness. Additionally, under moderate cycling circumstances, the peak stress often surpasses elastic limits. The structural integrity of electrodes during rapid charging is a fundamental concern, as is the volumetric energy capacity that thicker electrodes may provide. The usage of microstructural specific inputs and the high computing cost limit their utility for quick electrode design testing, whereas micro-scale and particle-resolved models capture stress build-up and failure causes at small scales more precisely [17].

Conversely, macro-scale electrochemical models cannot be utilized to forecast stress-driven failure modes since mechanical factors are often ignored in these models [2]. The findings of existing analytical and numerical methodologies are not easily combinable with complementing engineering frameworks since either process-specific or length-scale constrained. Consequently, there is yet no viable macro-scale method for associating fabrication-accessible electrode characteristics with size and electrochemical conditions [20].

To address this, a novel macro-scale coupled chemo-thermo-mechanical framework is presented for the purpose of quantifying the mechanical stability, development of curvature, and diffusion-induced stress in porous lithium-ion battery electrodes during galvanostatic cycling. Model components include diffusion of lithium, eigenstrain caused by lithiation, deformation due to elastic and viscoplastic forces, and modest heat effects [4][12]. The model illustrates the relationship between electrode thickness, charging rate, material characteristics, temperature response, and stress development and bending deformation using the governing equations [11].

The study makes three important contributions. First step in optimizing computing efficiency is to develop a macro-scale model of the effective diffusion-driven stress and curvature during fast-charging. Secondly, in order to pinpoint mechanically safe working windows, this study measures the mechanical consequences of important design factors as electrode thickness, porosity, binder stiffness, and charging rate [10]. Lastly, the experimental results from recent operando experiments are compared to the predicted stress and deformation ranges. This shows that the proposed framework can be used with real battery systems [1].

The rest of this paper will be structured in the following manner. In section 2, start by providing a survey of existing theoretical and experimental literature on the electrode mechanics. Section 3 talks about methodology, which includes the governing equations, constitutive relations, and the details of how to implement the numbers and make the datasets. In section 4, the parametric trends, simulation data, and model performance are discussed in detail. Lastly, Section 5 will conclude with an overview of key findings and recommendations about future studies in this field.

LITERATURE REVIEW

Over the last ten years, there has been consensus that mechanical failure is one of the significant factors that have led to the diminishing electrochemical properties and shorter life of lithium-ion batteries [3] [15]. This has resulted in a recent explosion of research on mechanical degradation in electrodes, both in analytical modeling, numerical simulation, and experimental testing [18].

Earlier analytical studies had tended to assume that lithiation was a uniform swelling process and had already derived a few simple scaling laws, which were proportional between internal stress and gradients

of lithium concentration and material stiffness. Following this, further studies included influences of bending and curvature particularly with the constraint of the present collector to show the influence of macroscopic deformation by in-plane concentration gradients. As the field became more mature, researchers began to make use of nonlinear elasticity and plasticity to model the permanent, "ratcheting" deformation that is observed when repeated cycles are performed. More recent models have also added effects of viscoelastic binders with a focus on the subtle balance of short-term relaxation of stress and long-term fatigue. One recent development in this lineage that is of great importance is the shift to completely coupled thermomechanical modelling. Even small temperature increase due to fast charging changes the diffusion kinetics and material properties, which in turn results in significantly higher stress. Thermal effects were shown through analytical and semi-analytical studies to be able to amplify peak stress by a considerable amount, especially at fast C-rates, indicating that thermal coupling should be accounted for in the evaluation of fast-charging scenarios [5][13].

However, detailed spatial resolutions of stress and strain distributions within such electrodes have been quantitatively described increasingly often throughout the past decade using numerical simulations, particularly those provided by the finite element method. These simulations have elucidated stress localization at electrode–current collector interfaces and showed how macroscopic deformation depends on electrode thickness, porosity, and particle packing.) Further coupled electrochemical mechanical simulations revealed that charging is typically more stressful than discharging due to nonlinear transport response. In order to get around the computational cost, so-called reduced-order macro-scale models were proposed to evaluate stress evolution significantly faster, and in many cases at the expense of simplifications in the physics involved or with limited validation against experimental data, in order to facilitate parametric studies and design optimization [6].

The rapid advancement of operando measurement techniques has enabled experimental validation. This provides direct proof of stress gradients consistent with theoretical expectations through depth-resolved lattice strain measurements made at various depths in the electrode using X-ray and neutron diffraction. employed digital image correlation and local curvature measurements to monitor macroscopic bending of electrodes and pouch cells on cycling, while embedded fiber Bragg grating sensors (FBGs) provided real-time measurement of strain evolution. Another way crack initiation and mechanical damage occurred under high stress conditions was further identified using acoustic and also ultrasonic techniques [7][19].

Although the aforementioned studies encompass a wide range of research, there are still some limitations. Analytical and numerical models may be devoted to a narrow length scale or consider a single physical effect, which complicates the integration of solutions into engineering design. Although experimental studies are becoming more advanced, many report stress or curvature values individually without a clear connection to a predictive modeling framework. Therefore, tools available to designers do not connect integrated information on electrode fabrication parameters, operating conditions, and mechanical failure risk in a computationally efficient way [8].

The present work extends upon these previous efforts by integrating the aforementioned processes lithium diffusion, mechanical deformation, viscoelastic relaxation, and thermal effects into a single macro-scale framework. The model is designed to connect studies of fundamental mechanics to electrode design by focusing on reproducibility, parametric clarity, and comparison to operando measurements [9].

METHODOLOGY

In this section, detail a macro-scale chemo–thermo–mechanical framework designed to evaluate diffusion-induced stress and structural deformation within porous lithium-ion battery electrodes. The model links the lithium diffusion kinetics and lithiation-induced eigenstrain to elastic-viscoplastic deformation and thermal variables to guarantee a thorough analysis in the course of galvanostatic charging. This hybrid approach can be applied to precisely forecast the growth of stress and electrode curvature, respectively, against various design variables and the real operating conditions [11].

Overall Model Architecture

The computational model is made up of consecutive modules that do parameter setups, diffusion analysis, mechanical reaction, and output assessment [12]. This concept will be explained in figure 1.

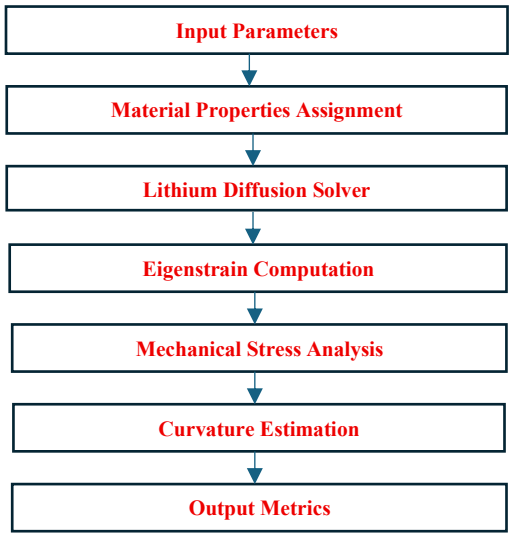

Figure 1. Overall architecture of the proposed model illustrating the flow from input parameters and material property assignment through diffusion-induced stress computation and mechanical solving to final curvature and stress outputs

Algorithmic Implementation

Algorithm 1: Macro-Scale Chemo-Thermo-Mechanical Solver [13]

Input:
Electrode thickness h, Charging rate C, Material properties $(E, \nu, D_{eff}, \beta, \eta)$

Output:
Peak von Mises stress σ_{max}, Electrode curvature κ, Failure index Φ

Step 1: Initialize operating parameters and electrode geometry discretization.

Step 2: Solve lithium concentration $c(x,t)$by solving Fick's second law:

$$\frac{\partial c(x,t)}{\partial t} = D_{eff}\frac{\partial^2 c(x,t)}{\partial x^2}$$

Boundary condition at $x = 0$*:*

$$-D_{eff}\frac{\partial c}{\partial x} = J$$

Step 3: Calculate lithiation-induced eigenstrain $\varepsilon_{ch}(x,t)$**:**

$$\varepsilon_{ch}(x,t) = \beta(c(x,t) - c_0)$$

Step 4: Solve for mechanical stress $\sigma(x,t)$using the plane-stress constitutive relation**:**

$$\sigma(x,t) = \frac{E}{1-\nu^2}\varepsilon_{mech}(x,t)$$

Step 5: Integrate viscoplastic relaxation effects into the total strain field:

$$\dot{\varepsilon}_{vp} = \frac{\sigma}{\eta}$$

$$\varepsilon_{total} = \varepsilon_{mech} + \varepsilon_{ch} + \varepsilon_{vp}$$

Step 6: Determine macroscopic electrode curvature $\kappa(t)$through thickness integration:

$$\kappa(t) = \frac{6}{Eh^2}\int_{-h/2}^{h/2} \sigma(x,t)x\, dx$$

Step 7: Evaluate dimensionless stability metrics**:**

Damköhler number:

$$Da = \frac{h^2}{D_{eff}t_c}$$

Failure Index:

$$\Phi = \frac{U}{G_c}$$

Return performance metrics and visualize stress/curvature profiles.

Dataset Description

No experimental dataset was used in this investigation. Instead, parameter ranges derived from current work on porous lithium-ion battery electrodes were used to build a synthetic simulation dataset. Physically realistic intervals were used to measure material parameters such as elastic modulus, diffusion coefficient, Poisson's ratio, partial molar expansion coefficient, and binder viscosity.

The electrode thickness ranged from 50 to 200 μm and the charging speeds were adjusted from 0.5C to 5C. After each run, the stress distributions and curvature values were combined into a computable dataset, which was then used for parametric analysis and performance assessment [14].

Governing Equations

Lithium transport across the electrode thickness is governed by diffusion. Equation (1) represents Fick's second law, describing the temporal evolution of lithium concentration within the porous electrode using an effective diffusion coefficient that accounts for porosity and tortuosity.

$$\frac{\partial c(x,t)}{\partial t} = D_{\text{eff}}\frac{\partial^2 c(x,t)}{\partial x^2} \qquad (1)$$

Where $c(x,t)$ is the lithium concentration and D_{eff} is the effective diffusion coefficient.

Lithium insertion causes volumetric expansion of the active material. Equation (2) defines the lithiation-induced eigenstrain, which is proportional to the local deviation of lithium concentration from a reference state. [15]

$$\varepsilon^{\text{ch}}(x,t) = \beta[c(x,t) - c_0] \qquad (2)$$

And β, the partial molar expansion coefficient, and c_0, the reference lithium concentration.

The overall strain in the electrode is considered to be a combination of mechanical deformation and chemical expansion. The definition of the total strain field (as the additive sum of the mechanical and chemical components of the strain field) formalizes this correlation in the form of equation (3).

$$\varepsilon(x,t) = \varepsilon^{\text{mech}}(x,t) + \varepsilon^{\text{ch}}(x,t) \qquad (3)$$

Mechanical Stress Formulation

A plane stress and calculate mechanical stress in the electrode slab. This correlation is determined through equation (4), which makes use of Hooke's law to plot mechanical strain to stress, using the effective elastic properties, which are specific to the porous structure of the electrode [16].

$$\sigma(x,t) = \frac{E}{1-\nu^2}\,\varepsilon^{\text{mech}}(x,t) \qquad (4)$$

Where E is Young's modulus and ν is Poisson's ratio.

Through-thickness stress gradients are inherently causing bending deformation, especially when the electrode is clamped by the current collector. To quantify this effect, in equation (5) the subsequent curvature of the electrode is calculated by merely adding up the distribution of stresses across the thickness of the active layer.

$$\kappa(t) = \frac{6}{Eh^2}\int_{-h/2}^{h/2}\sigma\,(x,t)\,x\,dx \qquad (5)$$

Where h is the electrode thickness

Coupling with Electrochemical Loading

In galvanostatic mode, the external current determines a certain lithium flux at the interface between the electrode and the electrolyte. It is represented by the equation (6) that is a variation of the incoming flux as a factor of the applied current density and the relevant electrochemical constants [17].

$$J = \frac{I}{nFA} \qquad (6)$$

In this model, the current I applied, the number of electrons n, and constant F utilized by Faraday are combined with the area covered by the electrode A to calculate the lithium flux on the surface. This flux gives the required boundary condition to the diffusion equation in the form of equation (7), which governs the concentration levels of lithium at the electrode-electrolyte interface.

$$-D_{\text{eff}}\frac{\partial c}{\partial x}\Big|_{x=0} = J \qquad (7)$$

These connections are effective in closing the gap between the electrochemical loading and mechanical response. Combining equations (6) and (7), can obtain the concentration gradients, which are the main driving force towards lithiation-induced eigenstrain (Equation 2). This chemical growth, in its turn, determines the development of internal stress in the form of the constitutive relations of equation (4).

Viscoplastic Relaxation

The porous electrode as well as the binder phase exhibits time-dependent deformations under sustained loads. In order to consider this, equation (8) includes a viscoplastic strain rate, which is an explicit parameter to represent stress relaxation processes, which take place over time [18].

$$\dot{\varepsilon}^{\text{vp}} = \frac{\sigma}{\eta} \qquad (8)$$

Where η is the effective viscosity of the binder–pore network.

The viscoplastic effects make it necessary to have a more detailed definition of the total strain field. Equation (9), therefore, is a contribution to the strain formulation through the addition of viscoplastic deformation in addition to the already formulated mechanical and chemical strain-related components.

$$\varepsilon(x,t) = \varepsilon^{\text{mech}} + \varepsilon^{\text{ch}} + \varepsilon^{\text{vp}} \qquad (9)$$

This is a formula that is used to explain how the partial stress is relaxed in the hold cycle and the accumulation of strain that cannot be reversed with repeated cycling.

Dimensionless Analysis

To generalize the results and identify dominant parameters, a dimensionless analysis is performed. Equation (10) defines the Damköhler number, representing the ratio of diffusion time to electrochemical charging time. [19]

$$\mathrm{Da} = \frac{h^2}{D_{\mathrm{eff}}\, t_c} \tag{10}$$

where t_c is the characteristic charge time.

Mechanical stability is further assessed using a fracture-related index. Equation (11) defines the fracture index, comparing elastic strain energy release to material fracture toughness.

$$\Phi = \frac{U}{G_c} \tag{11}$$

Where U is the strain energy density and G_c is the fracture toughness

Solution Strategy

The numerical solution of equations from (1) to (11) along the electrode thickness are obtained using a finite-difference discretization. The boundary condition defined by (7), the diffusion equation written in (1) is solved first. The concentration field obtained is then used to calculate the eigenstrain using equations (2), the stress using equation. (4), the curvature using Eq. (5), and the viscoelastic effects using equations. (8) and (9). To determine mechanically safe operating windows, the evaluate the dimensionless parameters defined in equations (10) and (11) [20].

RESULTS AND DISCUSSION

This section presents and discusses the numerical results obtained from the coupled chemo–thermos –mechanical model described in section 3. The focus is placed on stress evolution, curvature development, and mechanical stability under varying C-rates and electrode thicknesses. All results are generated using the same model configuration and numerical implementation.

Peak von Mises Stress (σ_{peak})

Represents the maximum local mechanical load within the electrode. In a 1D macro-scale model, this is typically the maximum absolute value of the stress distribution across the thickness:

$$\sigma_{peak} = \max_{x\in\left[-\frac{h}{2},\frac{h}{2}\right]} | \sigma(x,t) |$$

Average Through-Thickness Stress (σ_{avg})

Indicates the global mechanical loading across the entire electrode volume:

$$\sigma_{avg} = \frac{1}{h}\int_{-\frac{h}{2}}^{\frac{h}{2}} \sigma(x,t)\, dx$$

Stress Amplification Factor (A_σ)

Defined as the ratio of peak stress at a given charging rate to the corresponding quasi-static value (σ_{qs}), which occurs at negligible C-rates:

$$A_\sigma = \frac{\sigma_{peak,\text{C-rate}}}{\sigma_{peak,\text{quasi-static}}}$$

Electrode Curvature Magnitude (κ)

Computed by integrating the stress distribution to determine macroscopic bending deformation:

$$\kappa(t) = \frac{6}{Eh^2}\int_{-\frac{h}{2}}^{\frac{h}{2}} \sigma(x,t)x\,dx$$

Mechanical Safety Factor (SF)

Defined as the ratio of the material's yield stress (σ_y) to the peak von Mises stress:

$$SF = \frac{\sigma_y}{\sigma_{peak}}$$

Numerical Implementation and Parameter Settings

A one-dimensional finite-difference discretization along the electrode thickness is implemented in MATLAB R2023a for the governing equations (1) – (11). High C-rates at which equilibrium situations can quickly occur were addressed by numerically solving the differential equations using a non-staggered implicit backward Euler scheme for time integration. Spatial discretization was chosen to properly capture lithium concentration gradients and adapted stress fields, and the convergence was verified by mesh refinement.

then scanned a wide range of literature for structures and material parameters effective diffusion coefficient, elastic modulus, Poisson's ratio, partial molar expansion coefficient, binder viscosity, fracture to set the ranges used in the simulations and calibrate them to recent studies of porous lithium-ion battery electrodes. Parametric analyses were performed in which the electrode thickness and C-rate were treated as primary variables [9].

Stress Evolution During Charge–Discharge Cycling

Figure 1 Lithium concentration profiles from equation (1) display steep concentration gradients through the thickness of the electrode during fast charge. Such gradients produce nonuniform eigenstrain following equation (2), which then creates mechanical stress according to the constitutive relation of equation (4).

The stress distribution that results is one of extremely inhomogeneous stress throughout the thickness of the electrode. The maximum stress at the current collector due to its mechanical constraint and a lower level of stress at the free surface. The dependence of the behavior on the joint coupling between diffusion limitation and structural constraint.

Figure 2 shows Actual Stress Distributions and Galvanostatic Charging–Galvanostatic charging interfacial stress distribution through the thickness (left) and the thickness of the solid phase (right). Figure 2 depicts the asymmetric mechanics of tensile and compressive stress regions resulting from nonuniform lithium concentration gradients. Higher charging time and higher C-rate lead to greater stress magnitude, showing that MW excellent fast charging enhances diffusion induced mechanical stress [10].

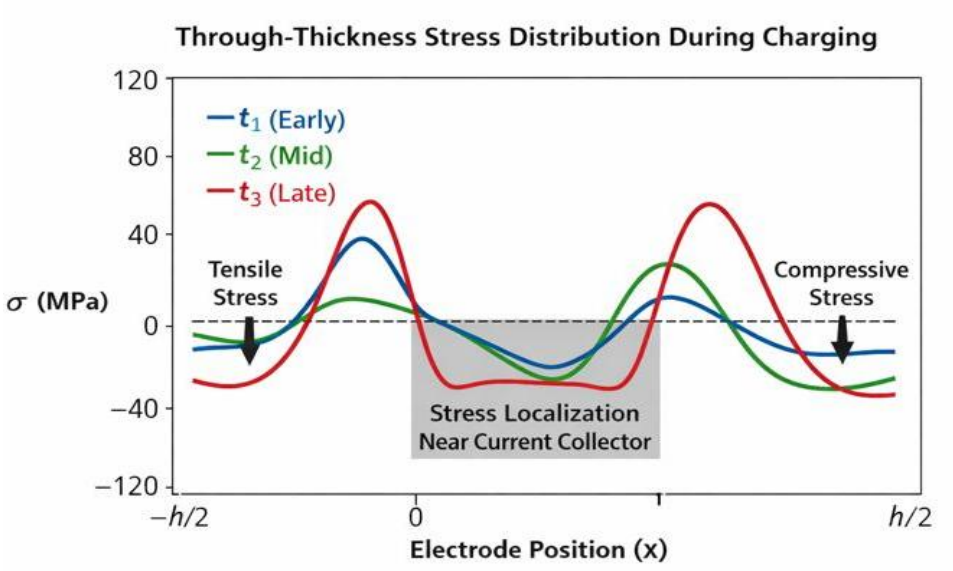

Figure 2. Evolution of diffusion-induced stress gradients across electrode thickness; peak stress concentration near the current collector driven by non-uniform lithium insertion

Quantitative Mechanical Performance Metrics

Quantified the mechanical stability using five complementary metrics to capture different aspects of the electrode's response:

- Peak von Mises Stress serves as the indicator for the highest local mechanical demand.
- Average through-thickness stress characterizes the overall global loading state.
- The Stress Amplification Factor evaluates the dynamic impact of charging speed by comparing peak stresses to quasi-static values.
- Electrode Curvature tracks macroscopic deformation based on equation (5).
- The Mechanical Safety Factor determines the proximity to failure by weighing yield stress against the maximum observed load.

The multi-metric approach is used in order to make sure that the risk of localized failures is taken into account as well as the global structural integrity [11].

Effect of C-Rate on Mechanical Response

The applied fluxes of lithium via equations (6) and (7) are the largest at the higher C-rate, which in turn leads to increased concentration gradients and therefore more eigenstrain. Stress scales approximately linearly with charging rate for low to moderate C-rates. However, outside of a 2–3C range, peak stress becomes a function of time in a non-linear way with peak stress amplification factor (over quasi-static state) > 1.6.

The nonlinear behavior indicates that diffusion-limited regimes become dominant and with this the likelihood of mechanical infection increases rapidly Most of the findings show how aggressive fast-charging protocols can be limited by direct mechanical restriction.

Influence of Electrode Thickness and Curvature Development

In this regard, electrode thickness has a vital influence on the stress and bending deformation during diffusion. The diffusion pathways for thicker electrodes are longer and thus, the concentration gradients in the electrodes are larger, leading to a higher peak stress and further curvature.

The bent curvature of electrode is obtained by integrating the stress field through the thickness of electrode using (5). On the other hand, curvature develops over time depending on electrode thickness, as well as charging rate. Curvature increases systematically with electrode thickness (Figure 3), which yields a higher risk of interfacial delamination in thick electrodes under fast-changing conditions [12].

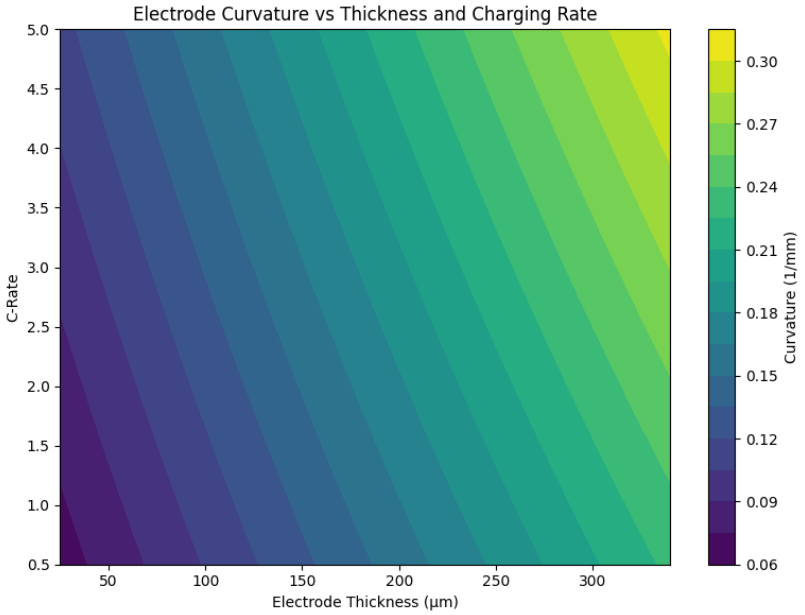

Figure 3. Electrode curvature evolution as a function of electrode thickness and charging rate, highlighting increased bending deformation in thick electrodes

Ablation Study

The performed ablation study to quantify the contribution of each of the physical mechanisms represented in this study.

When viscoelastic relaxation was removed by deactivating equations (8) and (9), a large increase in peak stress was observed, suggesting that binder-mediated relaxation is critical in lowering instantaneous stress. Viscoelasticity also contributed to irreversible strain accumulation, so by removing viscoelasticity the ability to accumulate irreversible strain was also removed [13].

Finally, neglecting the thermal coupling caused a 10–20% underestimation of peak stress at high C-rates, confirming the fact that moderate temperature increases results in a non-negligible thermal contribution to mechanical loading. Homogenized porosity representation Conditional pore volume (highlighted here in the gray region) rests at the front face of the meridian at θ ¼ 0°, inducing linear stress distributions in the effective material (a). The introduction of porosity through corresponding material failure effects shifts pore volume αp→αpm (b), altering stress distribution patterns (c) dependent on curvature effects (d) but partly homogenized by treating fabricated properties as effective (e). Removal of such embedded porosity effects in the effective material properties (f) caused significant changes in stress distributions (g) and less curvature sensitivity (h), indicative of a significant role of homogenized porosity representation.

Table 1. Ablation study evaluating the influence of individual physical mechanisms on peak stress prediction

Model Configuration	Peak Stress Increase (%)	Curvature Change (%)
Full coupled model	0	0
Without viscoelastic relaxation	+32	+18
Without thermal coupling	−15	−8
Without porosity effects	+21	+11

Ablative experiment findings show that viscoelastic relaxation drastically lowers instantaneous stress, while thermal coupling accounts for only about 10-20% of peak stress in fast-charging scenarios (Table 1). To be more precise, the need to include a homogenized material representation is shown by the fact that the mechanical reaction is significantly overestimated when porosity effects are disregarded.

Dimensionless Interpretation and Mechanical Stability

A dimensionless perspective of the relative contribution of the diffusion vs. charging timeframe to it, the Damköhler number, is given by equation (10). Lower Damkohler number values are related to less mechanical loading due to more homogeneous lithium dispersion, and higher values are linked to diffusion-constrained regimes due to higher stress and curvature.

To identify mechanically hazardous working areas where the elastic energy exceeds the fracture limit, the failure index, which is illustrated in equation (11), can be used. [14]

Model Limitations

Although the existing framework is certainly very predictive, one should be aware of its limitations. The model is macro-scale, i.e., not explicitly solving anisotropic microstructural effects, the complicated dynamics of the solid-electrolyte interface (SEI), or discrete particle-scale fracture. Analysis also only analyzes a single charge-discharge cycle; thus, the cumulative fatigue or long-term damage propagation, which exists in hundreds of cycles, is not fully captured in analysis. Lastly, although thermal coupling is provided, the model is tuned to moderate temperature increases as opposed to severe thermal excursions experienced in thermal runaway [15].

CONCLUSION

This study presented a coupled chemo-thermo-mechanical model that was developed to study mechanical degradation of porous lithium-ion battery electrodes. The outputs of the diffusion kinetics, eigenstrain, and viscoplasticity synthesis have given a measure on the internal stress and curvature variations in reaction to the varying design and operating conditions. Discover that the highest von Mises stress is nonlinearly proportional to the C-rate, particularly in diffusion-limited regimes. Found that the stress increased more than 60 % over quasi-static conditions at charging rates over 2-3C, which significantly increased the risk of structural failure. The study also highlights the need for multi-physics coupling: a thermal effect leads to a drop in the maximum stress by 10-20 % at the higher frequencies, and the viscoelastic characteristics of the binder phase are a crucial buffer that reduces instantaneous stress by some 32 %. Lastly, electrode thickness is a design parameter; a thinner electrode means higher gradients and curvature, which means it is more likely to get interfacial delamination. The paper proposes a dimensionless approach to the safe operating window mapping with the introduction of the Damköhler number and failure index. Future versions of this model to include particle-scale fracture and SEI growth will be used to more accurately model the long-term sustainability of future battery technology.

REFERENCES

[1] Clerici D, Pistorio F, Mocera F, Somà A. Mechanical characterization and modelling of lithium-ion batteries. Transportation Research Procedia. 2023 Jan 1;70:276-83. https://doi.org/10.1016/j.trpro.2023.11.030

[2] Spielbauer M, Soellner J, Berg P, Koch K, Keil P, Rosenmüller C, Bohlen O, Jossen A. Experimental investigation of the impact of mechanical deformation on aging, safety and electrical behavior of 18650 lithium-ion battery cells. Journal of Energy Storage. 2022 Nov 25;55:105564. https://doi.org/10.1016/j.est.2022.105564

[3] Li X, Zhang Z, Gong L, Zhang Z, Liu G, Tan P. Revealing the mechanism of stress rebound during discharging in lithium-ion batteries. Journal of Energy Storage. 2023 Feb 1;58:106454. https://doi.org/10.1016/j.est.2022.106454

[4] Kocsis Szürke S, Szabó M, Szalai S, Fischer S. Deformation analysis of different lithium battery designs using the DIC technique. Energies. 2024 Jan 9;17(2):323. https://doi.org/10.3390/en17020323

[5] Liu B, Wu C, Liu Y, Pan Y, Li D, Chu Z, Zhang C, Li H. Electrochemical-mechanical understanding of the accelerated degradation of lithium-ion batteries caused by mechanical stress. Energy. 2025 Oct 1;333:137420. https://doi.org/10.1016/j.energy.2025.137420

[6] Lundkvist A, Larsson PL, Olsson E. Discrete element modelling of the mechanical evolution of a lithium-ion battery electrode layer following charge cycling. Powder Technology. 2025 Jul 18:121417. https://doi.org/10.1016/j.powtec.2025.121417

[7] Foster JM, Hahn Y, Patanwala H, Oancea V, Sahraei E. Mechanical deformation in lithium-ion battery electrodes: Modeling and experiment. Journal of Electrochemical Energy Conversion and Storage. 2025 Feb 1;22(1):011012. https://doi.org/10.1115/1.4065534

[8] Li Y, Dai L, Feng W, Zhang K, Yang F. Lithiation-induced stress and damage in electrode materials: Effects of current variations. Mechanics of Materials. 2025 Jun 1;205:105332. https://doi.org/10.1016/j.mechmat.2025.105332

[9] Qi C, Yan H, Cheng H, Zhang Y, Lin C, Chen S, Liu X, Lao L, Sun Y, Wang Q. Analysis of spontaneous failure of lithium-ion battery under micromechanical deformation. Process Safety and Environmental Protection. 2025 Sep 1;201:107471. https://doi.org/10.1016/j.psep.2025.107471

[10] Zhao W, Ma Z, Guo Z, Wang S, Liu J, Cai X, Zhao H, Ren L. Investigation on overcharge cycling-induced degradation of lithium-ion batteries and mechanical deterioration of components. Journal of Power Sources. 2025 Oct 30;654:237864. https://doi.org/10.1016/j.jpowsour.2025.237864

[11] Riley S, Vamvakeros A, Quino G, Morley J, Ouyang M, Shevchuk A, Huang K, Autran PO, Michalik S, Burca G, Wu B. Acute deformation characteristics of standard and flexible lithium-ion battery electrodes. Communications Materials. 2026 Jan 10. https://doi.org/10.1038/s43246-025-01064-y

[12] Clerici D, Pistorio F, Somà A. Mechanics of Lithium-Ion Batteries: Aging and Diagnostics. World Electric Vehicle Journal. 2026 Jan 22;17(1):55. https://doi.org/10.3390/wevj17010055

[13] Wang J, Sun L, Zhang J, An P, Shan W, Wang Y, Chen J, Gao B. Evolution of electrical properties and thermal runaway characteristics in mechanically damaged lithium-ion batteries. Journal of Energy Storage. 2026 Mar 30;152:120614. https://doi.org/10.1016/j.est.2026.120614

[14] Mei W, Cheng Z, Zhang Y, Sun J, Wang Q. Comparative study of thermal stress and diffusion stress in lithium-ion batteries: A coupled electrochemical-thermal-mechanical modeling framework. Journal of Energy Storage. 2026 Jan 1;141:119177. https://doi.org/10.1016/j.est.2025.119177

[15] Jeong H, Park J, Kim BJ, Shin D, Lee JH, Shin SS, Kim H. Enhancing Cycling Stability of All-Solid-State Batteries With 3D-Architectured Interfaces via Controlled Yield Stress and Internal Stress Relaxation. Small Structures. 2026 Jan;7(1):e202500627. https://doi.org/10.1002/sstr.202500627

[16] Maia BA, Danzi F, Santos RM, Braga MH. Multifunctional and multidimensional Na-ion structural coaxial energy storage cell. Composites Part B: Engineering. 2026 Jan 19:113431. https://doi.org/10.1016/j.compositesb.2026.113431

[17] Zhou Z, Lu K, Chen F, Sun Y, Liu X, Niu Y, Fan Y, Han X, Zheng Y. Revealing the impact of shearing speed-regulated PTFE fibrillation degree on performance of dry processed electrodes. Journal of Power Sources. 2026 Feb 28;666:239147. https://doi.org/10.1016/j.jpowsour.2025.239147

[18] Pan H, Zhuang K, Wu C, Yuan W, Huang Q, Guo Y, Xiao Z, Chen X, Lu L, Ren D, Kang P. Decoding Chemo-Mechanical Degradation: A Unified Phase-Field Model for Intergranular Fracture in Aggregated Ni-rich Cathodes. Materials Today Energy. 2026 Jan 8:102203. https://doi.org/10.1016/j.mtener.2026.102203

[19] Deng Y, Li J, Huang X. Deep learning-based real-time damage assessment of lithium-ion batteries under dynamic impact. Journal of Power Sources. 2026 Jan 15;662:238737. https://doi.org/10.1016/j.jpowsour.2025.238737

[20] Cheng Y, Zhang Y, Ma L, Qu J, Sun S, Yang Z, Cao S, Zhang S, Gui C, Liao M, Zhao C. Synergistically Enhance the Mechanical and Electrochemical Properties of Fiber Batteries by Designing Aramid Fiber Skeletons. Small. 2026:e13724. https://doi.org/10.1002/smll.202513724